

Free Space Optical Cooperative Communications via an Energy Harvesting Harvest-Store-Use Relay

Chadi Abou-Rjeily, *Senior Member IEEE*, and Georges Kaddoum, *Member IEEE*

Abstract—In this paper, we consider a three-node free space optical (FSO) cooperative network with an energy harvesting (EH) decode-and-forward (DF) relay. The relay is equipped with an energy buffer and implements the harvest-store-use (HSU) architecture where the harvested energy is accumulated and used for forwarding the information from the source node to the destination node. We propose a novel HSU-based relaying strategy based on the simultaneous lightwave information and power transfer (SLIPT) concept where the relay harvests energy from the optical signal transmitted by the source. Firstly, we analyze the performance of the considered system by modeling the energy buffer as a continuous-space Markov chain (MC) for the sake of deriving the limiting distribution of the stored energy. Secondly, we discretize the state space and use the resulting discrete-space MC to derive the steady-state distribution of the buffer content. Thirdly, we propose an approximate discrete-space MC for capturing the energy buffer dynamics in a simple manner. The third approach is useful for relating the outage probability to the channel coefficients and average amounts of harvested energy in a simple closed-form manner. Simulation results validate the presented analytical evaluation and demonstrate the performance improvement that is achieved by the proposed scheme.

Index Terms—Free space optics, relaying, energy harvesting, dual-hop, cooperation, Markov chain, outage analysis.

I. INTRODUCTION

Relaying plays a vital role in enhancing the throughput, boosting the reliability, improving the diversity gains and extending the coverage of wireless networks whether in the context of radio frequency (RF) or free space optical (FSO) cooperative communications. Conventionally, relays are assumed to be battery-powered and, consequently, are readily available for assisting a source node (S) in its communications with a destination node (D) [1]. Recently, there has been a surge of interest in relays that are powered by energy harvesting (EH) as a means of prolonging the lifetime of energy-constrained networks [2]. Cooperative solutions have been included in recent wireless standards and their importance has been outlined in the imminent 5G networks with an extended field of applications including dense networking, Device-to-Device (D2D) communications, Vehicle-to-Vehicle (V2V) communications and Internet-of-Things (IoT) [3]. Due to the exponentially increasing number of deployed wireless devices, 5G must ensure energy efficiency in addition to

guaranteeing high-speed reliable communications at low cost. As such, the main motivation behind EH and relaying is to provide energy efficiency and spectral efficiency for next generation wireless networks [3]. Energy can be harvested from the ambient RF and optical signals, through the well studied simultaneous wireless information and power transfer (SWIPT) technique [4] and through the emerging simultaneous lightwave information and power transfer (SLIPT) method [5]. The SWIPT and SLIPT solutions exploit the capability of RF and optical signals, respectively, to simultaneously carry energy and information.

In RF networks, the vast majority of the recent EH schemes are based on the harvest-store-use (HSU) architecture [6]–[14]. For this architecture, the harvested energy is stored in an energy storage device, also referred to as energy buffer (such as a rechargeable battery or super-capacitor), and subsequently used for information transmission. Point-to-point (P2P) wireless powered communications were studied in [6], [7] where the RF energy harvested in the downlink is accumulated and used for transmitting the information along the uplink in a frequency division setup. The main difference between [6] and [7] resides in the manner in which the energy buffer is operated when the stored energy is less than the required transmit energy. In this case, the mobile node refrains from transmission in [6] while it transmits with whatever available energy in [7]. Three-node cooperative RF networks comprising a single EH-relay (R) were considered in [8], [9]. Incremental and non-incremental relaying were studied in [8] assuming a constant transmit power and an infinite-size energy buffer. Unlike non-incremental relaying, the signal might not be transmitted along the indirect S-R-D link with incremental relaying if the quality-of-service (QoS) is met along the direct S-D link. Decode-and-forward (DF) relaying with a maximal ratio combining (MRC) receiver was examined in [9] with a finite-size buffer with either fixed or variable transmit power from the relay. The performance analysis in [6]–[9] was based on studying the energy storage process by modeling the single energy buffer as a discrete-time continuous-space Markov chain. In this context, the limiting distribution of the stored energy was derived for Rayleigh fading environments that entail a tractable exponential distribution on the incoming harvested energy. In fact, for RF signals, the harvested energy is proportional to the squared magnitude of the channel coefficient.

Three-node RF DF networks were also studied in [10] with a greedy switching policy where R transmits a variable power level that is sufficient for ensuring data decodability at D. The single-relay scheme in [10] was further extended to multi-

C. Abou-Rjeily is with the Department of Electrical and Computer Engineering of the Lebanese American University (LAU), Byblos, Lebanon. (e-mail: chadi.abourjeily@lau.edu.lb).

G. Kaddoum is with the LACIME Laboratory, ÉTS Engineering School, University of Québec, Montreal, Canada (e-mail: georges.kaddoum@etsmtl.ca).

relay setups in [11], [12] where relay selection strategies were investigated based on partitioning the relays into two subsets. Relays in the first subset switch to the EH mode while relays in the second subset cooperate for forwarding the message to D based on a distributed beamforming scheme. In [11], [12], the decodability subset comprises the relays that were capable of decoding S's signal and that have enough stored energy. Unlike [6]–[9] that derived the continuous probability density function (pdf) of the continuous-space Markov chain, the performance analysis in [10]–[12] was based on discretizing the state space and deriving the discrete steady-state distribution of the discrete-space Markov chain. This calculation methodology was also adopted in [13] for studying amplify-and-forward (AF) relay selection with finite-size energy buffers and in [14] for tackling the physical layer security in two-hop RF networks. While the continuous approach ensures exact results, the discrete approach yields approximate results with a high level of accuracy if a large number of states is considered [10]. However, the continuous approach might not be culminated by closed-form expressions of the pdf especially for involved EH models and/or relaying protocols [8], [9]. Finally, for the discrete approach, it is hard to derive the steady-state distribution in closed-form if, for the sake of accuracy, discretization is performed over a large number of energy levels [10].

While EH from the RF signals for wireless powered cooperative communications has been well investigated over the last decade [2], there has been a recent growing interest in EH from light signals in the context of indoor visible-light communications (VLC) and outdoor FSO infrared communications [5]. This EH from the optical signals can be realized through dedicated optical wireless power transfer solutions [15], [16] or through the emerging SLIPT technique [5]. In [15], a dedicated unmodulated ground-based laser was used to deliver optical energy to charge an unmanned aerial vehicle (UAV) in flight. A similar application was outlined in [16] in the context of P2P communications where a FSO transmitter with permanent power supply communicates with a receiver with no power supply. Unlike [15], [16], the SLIPT strategy revolves around the simultaneous information transmission and power transfer. In fact, optical signals comprise a DC component that limits the modulation to the linear output-versus-input region of the optical source as well as an information-carrying alternating current (AC) component. The SLIPT concept revolves around solar panel based receivers where the DC and AC components of the received optical signal are separated and used for EH and information decoding, respectively. SLIPT-based P2P communications for amplitude modulated indoor VLC systems and pulse position modulated outdoor FSO systems were analyzed in [5], [17] and [18], respectively. Additionally, in the context of P2P communications, collaborative RF/VLC networks were considered in [19] where the optical transceivers implement the SLIPT strategy while a RF access point delivers complementary RF wireless power transfer. FSO EH was also considered in [20] with mixed FSO/RF communications where a ground base station delivers information and power to a UAV based on the SLIPT concept while the UAV communicates with a number of ground users over orthogonal RF channels. In [20], an optimization problem was formulated and solved

with the objective of maximizing the bit rate delivered to the worst ground user.

Despite the extensive literature on RF cooperative communications with HSU EH relays [6]–[14], to the authors' best knowledge, the use of relays possessing EH and energy storage capabilities was never considered before in FSO networks. In fact, the use of relays was not considered in [5], [15]–[19] that tackled optical EH with P2P noncooperative communications with a destination that is not equipped with an energy storage device. Although [20] considered the use of a UAV as a relay (that receives FSO signals and transmits RF signals), no energy storing capabilities were considered in this reference as well. Motivated by the above observations, this work targets FSO relaying with an EH relay that is equipped with an energy buffer. The design of such cooperative FSO systems cannot be readily borrowed from the existing literature on RF relaying [6]–[14] given the unique particularities that distinguish FSO systems from their RF counterparts. (i): FSO transmissions are based on narrow laser beams and, hence, are highly directive in nature. This implies that multiple FSO transmissions can take place simultaneously in the network with no interference where this feature can be exploited for enhancing the QoS of the network. Therefore, unlike the RF relaying solutions in [8]–[14], S can simultaneously communicate different signals to R and D in FSO networks. (ii): FSO relays operate naturally in the full-duplex mode. In fact, unlike RF systems where the same antenna is used for reception and transmission at R, a FSO relay can simultaneously receive signals at its photo-detector and transmit signals from its laser. In this context, all the RF relaying systems in [8]–[14] deploy half-duplex relays. In addition to adapting the relaying/EH strategy to the specificities of the FSO networks, additional challenges arise in the performance evaluation compared to RF systems. (i): Unlike RF signals where the harvested energy is proportional to the transmitted energy, more complicated non-linear EH models need to be adopted with optical signals [5]. (ii): RF relaying is widely analyzed over Rayleigh fading channels with the favorable implication that the harvested energy will follow the tractable exponential distribution [6]–[9]. In FSO systems, more complicated channel models must be considered thus adding to the complexity of the analysis.

The major contributions of this work are as follows:

- Propose a novel DF relaying strategy for single-relay FSO systems with a HSU EH relay. (i): Unlike the existing FSO EH networks [5], [15]–[20], we consider the case where the relay is equipped with an energy buffer. (ii): Unlike the existing RF EH networks [8]–[14], the proposed scheme takes into consideration the full-duplex capabilities at R as well as the high directivity of the FSO links. (iii): Unlike [6]–[14] that are based on a linear EH model over Rayleigh channels, we consider a nonlinear EH model over FSO gamma-gamma fading channels. (iv): Unlike most prior works [10]–[14], we do not ignore the S-D link. (v): Unlike [10]–[14] where the relay switches between the EH and information forwarding modes, we consider the possibility of simultaneous information reception and EH at R based on the SLIPT technique.

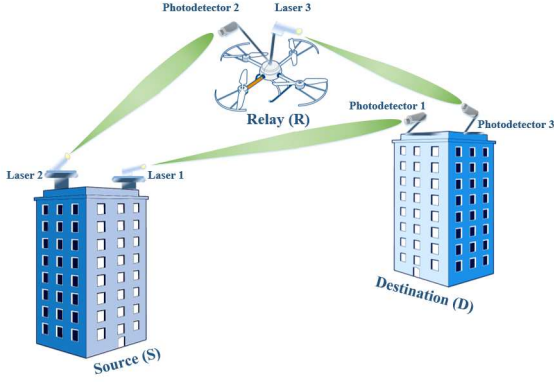


Fig. 1. Three-node cooperative FSO network.

- We analyze the performance of the proposed scheme by modeling the energy storage process as a continuous-space Markov chain in a way that is analogous to [6]–[9]. However, unlike [6]–[9] that hold for an exponentially distributed EH model, the presented performance analysis is tailored to the nonlinear EH model over gamma-gamma channels.
- We also carry out the performance analysis by discretizing the state space resulting in a discrete-space Markov chain analysis.
- While the above two calculation methods accurately capture the performance of the studied system, it is difficult to draw intuitive insights on the system performance based on these approaches in coherence with the existing literature [6]–[14]. As such, an approximate performance analysis is also provided based on narrowing down the admissible transitions in the discrete-space Markov chain. This approach results in simple closed-form expressions of the buffer content steady-state distribution as well as the system outage probability.

II. SYSTEM MODEL

A. Basic Parameters and Channel Model

Consider a three-node cooperative FSO network composed of a source (S), relay (R) and destination (D). Based on the non-broadcast highly-directive nature of the FSO transmissions, the communication between any pair of nodes takes place along a dedicated FSO link comprising an optical transmitter (laser) and an optical receiver (photo-detector) as highlighted in Fig. 1. Consequently, S is equipped with two lasers; one directed towards D and the other towards R. Similarly, D is equipped with two photo-detectors for reception along the S-D and R-D links while R is equipped with a laser and a photo-detector.

The three deployed lasers are assumed to operate under a peak power constraint where the transmitted optical power cannot exceed a maximum power level denoted by P_m (W). The modulation of the lasers is limited to the linear output-versus-input operating region where the generated optical power is proportional to the input driving current. Hence, the required electrical power is proportional to the square of the

optical power. Similarly, the optical-to-electrical conversion is limited to the linear region of the photo-detectors. Therefore, the received electrical current will be proportional to electrical current driving the transmitting laser.

We consider non-coherent optical communications with intensity modulation and direct detection (IM/DD). Non-negative Q -ary Pulse Amplitude Modulation (PAM) is implemented where the q -th symbol is modulated by pulsing the laser at the optical power p_q where $0 \leq p_1 < \dots < p_Q \leq P_m$. In particular, for the popular On-Off-Keying (OOK) scheme, $Q = 2$ with $p_1 = 0$ and $p_Q = P_m$. The S-D, S-R and R-D links will be denoted by link-1, link-2 and link-3, respectively. From Fig. 1, the i -th link extends from laser- i to photo-detector- i that are separated by a distance d_i for $i = 1, 2, 3$. When laser- i is pulsed at the modulated power $x_i \in \{p_1, \dots, p_Q\}$, the received electrical signal at photo-detector- i can be written as [1]:

$$y_i = \eta h_i^{(0)} h_i x_i + z_i, \quad (1)$$

where it is assumed that the three photo-detectors have the same responsivity η (A/W). In (1), z_i is the zero-mean real additive white Gaussian noise (AWGN) at photo-detector- i with variance σ^2 that is independent of the transmitted signal [1].

In this work, we adopt a channel model that takes into account the combined effects of path loss (the term $h_i^{(0)}$) as well as atmospheric turbulence-induced scintillation and misalignment-induced fading caused by pointing errors (combined in the term h_i). The path-loss term along link- i is obtained as [21]:

$$h_i^{(0)} = \frac{4S_r}{\pi\theta_d^2 d_i^2} e^{-\sigma_a d_i} \quad ; \quad i = 1, 2, 3, \quad (2)$$

where σ_a , S_r and θ_d stand for the attenuation coefficient, receiving area and diffraction-limited beam angle, respectively, where it is assumed that all deployed photo-detectors are identical. The probability density function (pdf) of h_i was derived in [22] assuming gamma-gamma turbulence and a Gaussian spatial intensity profile falling on a circular aperture at the receiver:

$$f_i(h) = \frac{\alpha_i \beta_i \xi_i^2}{A_i \Gamma(\alpha_i) \Gamma(\beta_i)} G_{1,3}^{3,0} \left[\frac{\alpha_i \beta_i}{A_i} h \left| \begin{matrix} \xi_i^2 \\ \xi_i^2 - 1, \alpha_i - 1, \beta_i - 1 \end{matrix} \right. \right], \quad (3)$$

where $\Gamma(\cdot)$ is the Gamma function and $G_{p,q}^{m,n}[\cdot]$ is the Meijer G-function. In (3), α_i and β_i stand for the distance-dependent parameters of the gamma-gamma distribution:

$$\alpha_i = \left[\exp \left(0.49 \sigma_R^2(d_i) / (1 + 1.11 \sigma_R^{12/5}(d_i))^{7/6} \right) - 1 \right]^{-1}$$

$$\beta_i = \left[\exp \left(0.51 \sigma_R^2(d_i) / (1 + 0.69 \sigma_R^{12/5}(d_i))^{5/6} \right) - 1 \right]^{-1},$$

where the Rytov variance is given by $\sigma_R^2(d) = 1.23 C_n^2 k^{7/6} d^{11/6}$ with k and C_n^2 denoting the wave number and refractive index structure parameter, respectively [21], [22].

In (3), the parameters A_i and ξ_i are related to the pointing errors with $A_i = [\text{erf}(v_i)]^2$ where $\text{erf}(\cdot)$ stands for the error function with $v_i = \sqrt{\pi/2} (a_i / \omega_{z,i})$ where a_i is the radius of receiver- i and $\omega_{z,i}$ is the beam waist along the link- i .

$\xi_i = \omega_{z_{eq},i}/2\sigma_{s,i}$ where $\sigma_{s,i}$ stands for the pointing error displacement standard deviation at receiver- i and $\omega_{z_{eq},i}^2 = \omega_{z,i}^2 \sqrt{\pi} \operatorname{erf}(v_i) / [2v_i e^{-v_i^2}]$ [22].

B. Information Transmission

In [23], a lower bound was derived for the capacity of non-negative PAM optical communications with an additive Gaussian noise under a peak power constraint. For such channels, the capacity is maximized for an average-to-peak power ratio of 1/2: $\frac{1}{Q} \sum_{q=1}^Q p_q = \frac{P_m}{2}$. The bound on the achievable rate (in bits/s/Hz) is given by:

$$R_i = \frac{1}{2} \log_2 \left(1 + \left(\frac{\eta h_i^{(0)} h_i P_m / 2}{\sigma} \right)^2 \right). \quad (4)$$

For a target threshold rate of R_{th} , the communication link will be in outage if the rate R_i in (4) falls below R_{th} : $p_i \triangleq \Pr(R_i < R_{th})$. Following from (4), the outage probability can be determined according to the following relation [22], [24]:

$$p_i = \frac{\xi_i^2}{\Gamma(\alpha_i)\Gamma(\beta_i)} G_{2,4}^{3,1} \left[\frac{\alpha_i \beta_i \sigma \sqrt{2^{2R_{th}} - 1}}{A_i \eta h_i^{(0)} P_m / 2} \middle| \begin{matrix} 1, \xi_i^2 + 1 \\ \xi_i^2, \alpha_i, \beta_i, 0 \end{matrix} \right]. \quad (5)$$

Based on the above formulation, the target information rate cannot be met along the S-D, S-R and R-D links with probabilities $p_{SD} \triangleq p_1$, $p_{SR} \triangleq p_2$ and $p_{RD} \triangleq p_3$, respectively.

C. Energy Harvesting

S is assumed to have a fixed power supply while R is an EH node. In this context, R harvests energy from the light beam emitted by S (i.e. laser-2 in Fig. 1) and accumulates this energy in an energy buffer. The accumulated energy at R is then used for information forwarding to D. Such scenarios are often encountered in real life systems. One practical application corresponds to sensor networks where some nodes may be equipped with batteries that are periodically replaced or charged by the operator while the self-sustaining sensor nodes must harvest their energy from the surrounding environment similar to the FSO system model considered in [16]. In such scenarios, the harvested energy accommodates for the entire power consumption at the self-sustaining nodes. Another application corresponds to the case where S and D are ground stations that are connected to the power grid while R is a UAV with stringent power consumption constraints and battery lifetime [18], [20]. For such systems, charging the UAV's battery from a power beacon transmitted from a terrestrial laser charging station can sustain the UAV in its entire flight duration [25]. In this case, harvesting energy from a 100 mW modulated laser rather than a 10 W power laser (as in [25]) can increase the flight duration by 1%. Given that in practice a UAV is deployed to simultaneously serve multiple users in a wavelength division multiplexing (WDM) manner, then a moderate number of ten users can extend the flight duration by around 10%. Evidently, this number will be further increased MN -folds by deploying $M \times N$ optical arrays. Therefore, under nominal operating scenarios, the total

FSO harvested energy can sustain the UAV's propulsion for a significant fraction of its flight duration.

For solar panel-based receivers, optical EH can be realized in a simple and efficient manner by blocking the DC component of the received signal and passing it through the EH branch [5], [17]–[20]. For an average optical power of P_{av} transmitted from S to R, the harvested energy at R is given by [5]:

$$E(P_{av}) = fV_t I_{DC}(P_{av}) \ln \left(1 + \frac{I_{DC}(P_{av})}{I_0} \right), \quad (6)$$

where f , V_t and I_0 stand for the photo-detector's fill factor, thermal voltage and dark saturation current, respectively. In (6), $I_{DC}(P_{av})$ stands for the DC component of the output current:

$$I_{DC}(P_{av}) = \eta h_2^{(0)} h_2 P_{av}. \quad (7)$$

As will be highlighted in the next subsection, along the S-R link, P_{av} assumes one of the two values $P_{av} = P_m$ and $P_{av} = P_m/2$. The value $P_{av} = P_m$ corresponds to the case where S is transmitting an unmodulated signal with fixed power P_m to R where this value maximizes the harvested energy. The value $P_{av} = P_m/2$ corresponds to the case where S is transmitting an information-carrying modulated signal to R where this choice achieves the capacity in (4). Operating laser-2 in the linear region implies that the DC component of the current driving this laser is proportional to P_{av} in both cases. The selection of P_{av} is better illustrated in Fig. 2 that shows the flowchart of the relaying scheme.

The communication-related energy consumption at R comprises the energies expended for reception, signal processing and transmission. We assume that the energy needed for transmission (i.e. the energy needed to drive laser-3 in Fig. 1) constitutes the major source of communication-related energy consumption at R. In what follows, the transmission time will be normalized to unity and, hence, the terms power and energy will be used interchangeably throughout this paper.

D. Relaying Protocol

The implemented FSO DF relaying protocol based on the HSU architecture is as follows:

- S first attempts to transmit the information message directly to D along the S-D link. During this phase, since S is connected to a power supply (often the power grid), it also strives to transfer energy to R along the S-R link. This can be realized by simultaneously transmitting an unmodulated signal with the maximum power P_m from laser-2 directed from S to R as shown in Fig. 1. In this case, the harvested energy at R is $E(P_m)$ based on (6).
- If the transmission in the first phase along the direct link was successful (with probability $1 - p_{SD}$), S proceeds with the transmission of a new information message. Otherwise, the S-D link is in outage and S attempts to communicate the message through R. In this scenario, one of the two following cases arises. (i): The stored power at R falls below $P_m/2$. In this case, R does not have enough stored power to relay the message to D and, hence, switches to the EH mode. (ii): The stored energy at R

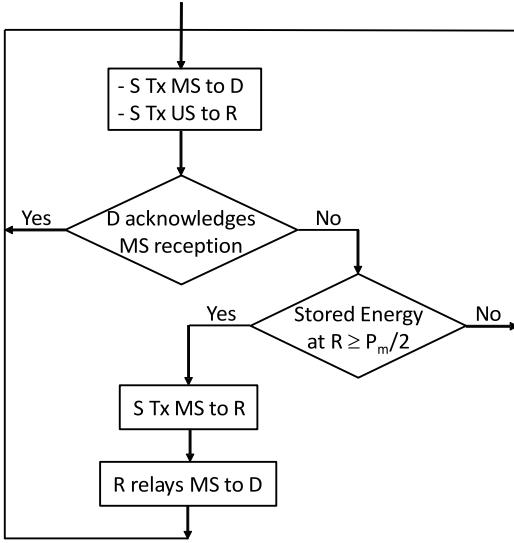


Fig. 2. Flowchart of the relaying protocol. MS stands for modulated signal ($P_{av} = P_m/2$) and US stands for unmodulated signal ($P_{av} = P_m$).

exceeds $P_m/2$. In this case, S communicates the message to R by transmitting a modulated signal with an average power of $P_m/2$. In its turn, R decodes the message and consumes a power $P_m/2$ to forward the message to D. In this case, optical energy can also be harvested from the information-carrying signal by feeding the DC component to the harvesting branch (SLIPT architecture) resulting in a harvested energy of $E(P_m/2)$ at R.

The relaying protocol is better described in Fig. 2. It is worth highlighting that the implementation of the proposed relaying strategy involves the transmission of a single feedback bit from R to S only when S attempts to communicate with R (i.e. the S-D link is in outage). This bit indicates whether the stored energy level at R exceeds $P_m/2$ or not. In the first case, S proceeds with the transmission of an information-carrying signal with average power $P_m/2$ while, in the second case, S transmits at the constant power level P_m to achieve maximum EH at R. In this context, the exchange of this feedback bit for a fraction p_{SD} of the time involves a marginal additional power consumption that can be safely neglected. This is especially true since practical communication systems often involve exchanging positive/negative acknowledgement (ACK/NACK) between the communicating nodes.

The implementation of a diversity combining scheme at D implicates that all information symbols must be transmitted along both the direct link S-D and the indirect link S-R-D. While this option is appealing for self-powered relays, it is not fully viable for EH relays that might not have a sufficient amount of stored energy to participate in the cooperation effort. Moreover, the continuous transmission from R will expend its battery at a faster pace which is not appropriate for EH relays. These observations motivate the proposed relaying strategy where, for the sake of energy efficiency that is of paramount importance in the considered system setup, only those information symbols that cannot be delivered along the direct link are relayed from R. Furthermore, this strategy

relaxes the synchronization constraints along the constituent links and avoids queuing and detection delays at D.

Denote by $B(i)$ the energy level in the energy buffer during the i -th signaling interval. Based on the implemented relaying strategy, the evolution of the energy buffer is captured by the following relation:

$$B(i+1) = B(i) + \begin{cases} E\left(\frac{P_m}{2}\right) - \frac{P_m}{2}, & \text{S-D link in outage \& } B(i) \geq \frac{P_m}{2}; \\ E(P_m), & \text{otherwise.} \end{cases}, \quad (8)$$

where, from (5), the S-D link is in outage with probability p_{SD} . In (8), without loss of generality, we assume that the energy buffer has an infinite size. This assumption is not limiting since the storage capabilities of modern storage devices are much higher than the amounts of harvested energy that are typically small. In fact, it can be observed that the optical wireless harvested energy in (6) takes very small values especially for long FSO links or under unclear weather conditions like fog and rain. This observation will be further discussed in Section IV.

III. PERFORMANCE ANALYSIS

A. Preliminaries

The outage probability of the relaying system with an EH relay can be written as:

$$P_{out} = p_{SD} \left[\Pr\left(B < \frac{P_m}{2}\right) + \Pr\left(B \geq \frac{P_m}{2}\right) [p_{SR} + p_{RD} - p_{SR}p_{RD}] \right], \quad (9)$$

where the system is in outage if the information message cannot be delivered neither along the direct link S-D (with probability p_{SD}) nor and along the indirect link S-R-D. It is recalled that, R will fail in forwarding the message if either (i): its energy level falls below the transmission level $P_m/2$ or (ii): it has enough energy but the link S-R-D is in outage. Finally, this latter link suffers from outage when either the S-R or the R-D hops are in outage.

The energy storage process in (8) is a discrete-time Markov chain over a continuous state space where the energy level B can assume any positive real value. The objective of this section is to derive the limiting pdf of the stationary distribution associated with the process $\{B(i)\}$. As highlighted in [6]–[9], the stationary distribution exists only if the energy buffer is stable. This stability is attained if the energy departure rate exceeds the energy arrival rate. In other words, the storage process in (8) possesses a stationary distribution if:

$$(1 - p_{SD})E[E(P_m)] + p_{SD}E[E(P_m/2)] \leq p_{SD}\frac{P_m}{2}, \quad (10)$$

where $E[\cdot]$ stands for the time-average operator. The condition in (10) avoids the overflow of the buffer ($B \rightarrow \infty$). This condition is derived assuming that there is enough stored energy in the buffer for transmission ($B \geq \frac{P_m}{2}$) since, otherwise, the buffer would contain a small amount of energy and would not risk energy overflow given the small amounts

of harvested energy. The quantity to the left-hand-side of (10) stands to the average amount of harvested energy where with probability $1 - p_{\text{SD}}$ (resp. p_{SD}) the S-D link is not in outage (resp. in outage) and, hence, R is harvesting an energy of $E(P_m)$ (resp. $E(P_m/2)$). The quantity on the right-hand-side of (10) stands to the average amount of expended energy since R is transmitting a power of $P_m/2$ when the direct link is in outage (always assuming that the buffer is close to overflow and $B \geq \frac{P_m}{2}$). It is clear that the condition in (10) holds especially for relatively long link distances under unfavorable weather conditions following from the fact that the wireless optical harvested energy will be small in such scenarios. Further discussions on this matter will be provided in Section IV.

On the other hand, if the stability condition in (10) does not hold, then after a finite number of time slots the Markov chain will tend to the absorbing state $B \rightarrow \infty$ (or fully charged battery). This implies that the transmission power level $\frac{P_m}{2}$ is always likely to be available for retransmitting the information from R [6]–[9]: $\Pr(B \geq P_m/2) \rightarrow 1$. In this case, the system simplifies to a conventional three-node network with a self-powered relay where, from (9), the corresponding outage probability is given by $P_{\text{out}} = p_{\text{SD}} [p_{\text{SR}} + p_{\text{RD}} - p_{\text{SR}}p_{\text{RD}}]$.

B. Limiting Distribution of the Energy Buffer: Continuous Approach

The optical wireless EH model in (6)-(7) differs substantially from RF EH where the harvested energy is proportional to the squared magnitude of the channel coefficient [6]–[14]. In this case, for Rayleigh fading channels, the harvested energy will follow the mathematically tractable exponential distribution. On the other hand, (6)-(7) highlight a highly non-linear dependence on a mathematically challenging gamma-gamma random variable. As such, the derivations presented in this section differ substantially from those provided in [6]–[9] for exponentially distributed RF harvested energy. Without resorting to discretizing the continuous state space, the stationary distribution can be determined according to the following proposition.

Proposition 1: For stable energy buffers, the limiting pdf of the stationary distribution of the energy buffer content is given by:

$$g(x) = \begin{cases} g_1(x) = a [1 - e^{-bx}], & 0 \leq x < \frac{P_m}{2}; \\ g_2(x) = ce^{-bx}, & x \geq \frac{P_m}{2}. \end{cases}, \quad (11)$$

where a , b and c are positive constants with:

$$a = \frac{2}{P_m}; \quad c = \frac{2}{P_m} \left[e^{b\frac{P_m}{2}} - 1 \right], \quad (12)$$

while b satisfies the following relation:

$$\frac{1}{(1 - p_{\text{SD}}) + p_{\text{SD}}e^{-b\frac{P_m}{2}}} = \int_0^{+\infty} f_E(t)e^{bt} dt. \quad (13)$$

In (13), $f_E(x)$ corresponds to the pdf of the harvested energy in (6) that can be accurately approximated by:

$$f_E(x) = \frac{1/\mu}{W\left(\frac{x}{\mu\nu}\right) + 1} f_2\left(\frac{x}{\mu W\left(\frac{x}{\mu\nu}\right)}\right); \quad x \geq 0, \quad (14)$$

where, from (6)-(7), $\mu \triangleq fV_t\eta h_2^{(0)}P_m$ and $\nu \triangleq \frac{I_0}{\eta h_2^{(0)}P_m}$. In (14), $W(\cdot)$ stands for the Lambert W-function while $f_2(\cdot)$ stands for the pdf in (3).

Proof: The proof is provided in Appendix A. \blacksquare

Based on proposition 1, the outage probability can be determined from (9) with:

$$\begin{aligned} \Pr\left(B \geq \frac{P_m}{2}\right) &= \int_{\frac{P_m}{2}}^{+\infty} g_2(x) dx = \frac{c}{b} e^{-b\frac{P_m}{2}} \\ &= \frac{2}{bP_m} \left[1 - e^{-b\frac{P_m}{2}} \right] = 1 - \Pr\left(B < \frac{P_m}{2}\right), \end{aligned} \quad (15)$$

following from (11) and (12) where the constant b is given in (13).

Note that while the solution provided in proposition 1 is highly accurate, its main limitation resides in the fact that the integral in (13) cannot be solved analytically given the complexity of the pdf in (14). Consequently, (13) needs to be solved numerically. While numerically solving this equation with one unknown is simple, the numerical method fails in relating the constant b , and hence P_{out} , to the system parameters in an intuitive and tractable manner.

C. Limiting Distribution of the Energy Buffer: Exact Discrete Approach

1) *Discretizing the Continuous State Space:* In order to overcome the aforementioned limitation associated with the intractability of the parameters of the limiting pdf in (11), we next resort to an exact discrete approach that is based on discretizing the continuous state space. This approach is widely adopted in the open literature as it yields accurate results if the total number of states is sufficiently large [10]–[14].

The energy interval $[0, \frac{P_m}{2}]$ will be discretized into $L + 1$ energy levels $\epsilon_i = i\Delta$ for $i = 0, \dots, L$ where $\Delta \triangleq \frac{P_m}{2L}$. The entire energy buffer (over the energy interval $[0, \frac{P_m}{2}]$) will be discretized into $L' + 1$ energy levels $\{\epsilon_i\}_{i=0}^{L'}$ with $L' \gg 1$ since an infinite-size energy buffer is considered. As such, the continuous-space Markov chain will be approximated by a discrete-space Markov chain over $L' + 1$ states denoted by $\{S_i\}_{i=0}^{L'}$ where the energy buffer is in state S_i when the stored energy is equal to ϵ_i . With the adopted discrete battery model, the amount of harvested energy can only be one of the discrete energy levels. Equivalently, the Markov chain will move to state S_j if the accumulated energy (stored energy plus harvested energy minus transmitted energy) falls in the interval $[\epsilon_j, \epsilon_{j+1}[$. In what follows, we fix $E \triangleq E(P_m)$ and $E' \triangleq E(P_m/2)$ in (8) for the sake of notational simplicity.

2) *Transition Probabilities:* In what follows, we denote by $p_{i,j}$ the transition probability of going from state S_i to state S_j . The following cases will be considered for evaluating the $(L' + 1)^2$ transition probabilities.

Case 1: $i \in \{0, \dots, L - 1\}$. In this case, the energy stored in the buffer falls below $\frac{P_m}{2}$ and, consequently, R cannot relay the message to D. Following from (8), R will enter the EH mode where its residual energy cannot decrease. Therefore:

$$p_{i,j} = 0; \quad j = 0, \dots, i - 1. \quad (16)$$

On the other hand, for $j = i, \dots, L' - 1$, the chain will move from state S_i to state S_j if the sum of stored and harvested energies falls in $[\epsilon_j, \epsilon_{j+1}]$:

$$\begin{aligned} p_{i,j} &= \Pr(\epsilon_j \leq \epsilon_i + E < \epsilon_{j+1}) \\ &= F_E((j - i + 1)\Delta) - F_E((j - i)\Delta) ; j = i, \dots, L' - 1, \end{aligned} \quad (17)$$

where $F_E(\cdot)$ is the cumulative distribution function (cdf) associated with the pdf $f_E(\cdot)$ in (14).

Finally, a transition to state $S_{L'}$ will occur if the sum of stored and harvested energies exceeds $\epsilon_{L'}$:

$$p_{i,j} = \Pr(\epsilon_i + E \geq \epsilon_{L'}) = 1 - F_E((L' - i)\Delta) ; j = L'. \quad (18)$$

Case 2: $i \in \{L, \dots, L'\}$ and $j < i$. In this case, R has enough stored energy for information transmission. Since the stored energy dropped ($j < i$), then it's not possible that R is in the pure EH mode. Therefore, in this case, R has definitely entered the information relaying (IR) mode which can happen only if the S-D link is in outage. Since R consumes an energy of $\frac{P_m}{2} = L\Delta = \epsilon_L$ for IR, then this energy consumption will result in a transition from state S_i to state S_{i-L} while the harvested energy E' cannot but increase the stored energy. Therefore:

$$p_{i,j} = 0 ; j = 0, \dots, i - L - 1. \quad (19)$$

On the other hand, for $j = i - L, \dots, i - 1$, state S_j can be reached from state S_i with the following probability:

$$\begin{aligned} p_{i,j} &= p_{SD} \Pr(\epsilon_j \leq \epsilon_i + E' - \epsilon_L < \epsilon_{j+1}) \\ &= p_{SD} [F_{E'}((j + 1 - i + L)\Delta) - F_{E'}((j - i + L)\Delta)] \\ &; j = i - L, \dots, i - 1, \end{aligned} \quad (20)$$

where $F_{E'}(\cdot)$ stands for the cdf of E' with $F_{E'}(x) = F_E(2x)$ as highlighted in Appendix A.

Case 3: $i \in \{L, \dots, L' - 1\}$ and $j \geq i$. In this case, since the stored energy increased, then one of the two following scenarios can hold given that R has enough energy for IR. (i): R is in the EH mode which arises if the S-D link is not in outage. (ii): R is in the IR mode and it had harvested more energy than it had expended for information transmission (the S-D link is in outage in this case). Therefore, for $j \neq L'$:

$$\begin{aligned} p_{i,j} &= (1 - p_{SD}) \Pr(\epsilon_j \leq \epsilon_i + E < \epsilon_{j+1}) \\ &\quad + p_{SD} \Pr(\epsilon_j \leq \epsilon_i + E' - \epsilon_L < \epsilon_{j+1}) \\ &= (1 - p_{SD}) [F_E((j - i + 1)\Delta) - F_E((j - i)\Delta)] \\ &\quad + p_{SD} [F_{E'}((j + 1 - i + L)\Delta) - F_{E'}((j - i + L)\Delta)] \\ &; j = i, \dots, L' - 1. \end{aligned} \quad (21)$$

Similarly, for $j = L'$:

$$\begin{aligned} p_{i,j} &= (1 - p_{SD}) \Pr(\epsilon_i + E \geq \epsilon_{L'}) + p_{SD} \Pr(\epsilon_i + E' - \epsilon_L \geq \epsilon_{L'}) \\ &= (1 - p_{SD}) [1 - F_E((L' - i)\Delta)] \\ &\quad + p_{SD} [1 - F_{E'}((L' - i + L)\Delta)] ; j = L'. \end{aligned} \quad (22)$$

Case 4: $i = j = L'$. This case is similar to case 3. Setting $i = L'$ in (22) results in:

$$p_{L',L'} = (1 - p_{SD}) + p_{SD} [1 - F_{E'}(L\Delta)]. \quad (23)$$

From (16)-(23), it can be easily verified that $\sum_{j=0}^{L'} p_{i,j} = 1$ for $i = 0, \dots, L'$. Finally, for a fine discretization ($\Delta \ll 1$), probabilities of the form $F_E((\delta + 1)\Delta) - F_E(\delta\Delta)$ tend to the value $\Delta f_E(\delta\Delta)$. The same holds if E is replaced by E' .

3) Steady-State Distribution and Outage Probability: From the transition probabilities, we construct the $(L' + 1) \times (L' + 1)$ state transition matrix \mathbf{P} whose (j, i) -th element is equal to $p_{i,j}$. The steady-state distribution vector π can be determined from \mathbf{P} as follows [10]:

$$\pi = (\mathbf{P} - \mathbf{I} + \mathbf{B})^{-1} \mathbf{b}, \quad (24)$$

where \mathbf{I} is the $(L' + 1) \times (L' + 1)$ identity matrix, \mathbf{B} is the $(L' + 1) \times (L' + 1)$ matrix whose elements are all equal to 1 and \mathbf{b} stands for any column of \mathbf{B} . In (24), $\pi = [\pi_0, \dots, \pi_{L'}]^T$ where π_i stands for the probability that the energy buffer is in state S_i at steady-state.

The steady-state distribution π is useful for evaluating the outage probability in (9). In fact, the probability $\Pr(B < \frac{P_m}{2})$ can be calculated as: $\Pr(B < \frac{P_m}{2}) = \sum_{i=0}^{L-1} \pi_i$.

Despite the high level of accuracy that can be achieved by the discretization approach for a large number of states and small discretization interval-size Δ , the main limitation of this method resides in the fact that it is very hard to evaluate the steady-state distribution in (24) in closed-form. In fact, for $L' \gg 1$, the state transition matrix \mathbf{P} has a large number of dimensions and the inversion of the matrix $\mathbf{P} - \mathbf{I} + \mathbf{B}$ does not relate the steady-state probabilities $\{\pi_i\}$ to the transition probabilities $\{p_{i,j}\}$ in a simple and intuitive manner. This is especially true since (17), (18), (21), (22) and (23) show that from each state S_i , the Markov chain can evolve to any other subsequent state S_j (for $j > i$) with a non-zero probability. Similarly, (16), (19) and (20) show that each state S_i is linked to L previous states S_j (for $j < i$) where L assumes large values if the interval-size Δ is to be kept small (since $\Delta = \frac{P_m}{2L}$).

D. Limiting Distribution of the Energy Buffer: Approximate Discrete Approach

In order to overcome the aforementioned limitation related to the excessively large number of possible transitions between the states of the discrete Markov chain, we next resort to a simplified approach that yields a tractable closed-form approximate solution.

Observation 1: It can be observed that the variance of the optical harvested energy in (6) is very small. This follows mainly from the presence of the logarithmic function and from the fact that I_0 assumes very small values. This observation will be further elaborated on in Section IV.

Following from observation 1, the performance analysis in this section will be based on the assumption that the harvested energy is almost constant and, hence, can be approximated by the corresponding average value. Therefore, in (8), we set $E(P_m) \approx \mathbb{E}[E(P_m)] = \int_0^{+\infty} x f_E(x) dx$ where the pdf $f_E(x)$ is given in (14). Similarly, we take $E(P_m/2) \approx \mathbb{E}[E(P_m/2)] = \int_0^{+\infty} 2x f_E(2x) dx$ following from Appendix

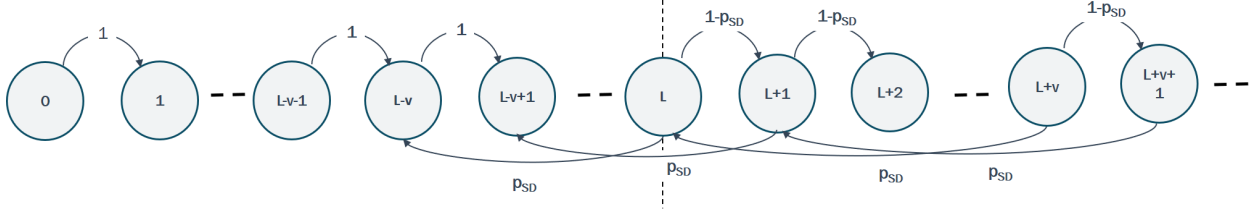


Fig. 3. The approximate discrete Markov chain based on observation 1.

A. Moreover, without any loss of generality, we select the energy step-size Δ of the discrete Markov chain as follows:

$$\Delta = \frac{P_m/2}{L} = \mathbb{E}[E(P_m)]. \quad (25)$$

Following from (25), the buffer evolution equation in (8) results in the following transition probabilities that describe the behaviour of the approximate discrete Markov chain:

$$p_{i,j} = \begin{cases} 1, & j = i + 1; \\ 0, & \text{otherwise.} \end{cases}, \quad i < L, \\ p_{i,j} = \begin{cases} 1 - p_{SD}, & j = i + 1; \\ p_{SD} & j = i - v; \\ 0, & \text{otherwise.} \end{cases}, \quad i \geq L, \quad (26)$$

where v is the constant positive rounded integer given by:

$$v = \frac{P_m/2 - \mathbb{E}[E(P_m/2)]}{\mathbb{E}[E(P_m)]} = \frac{P_m/2 - \mathbb{E}[E(P_m/2)]}{\Delta}. \quad (27)$$

In fact, in (26), when $i < L$ (and, hence, $\epsilon_i < \frac{P_m}{2}$), R is in the EH mode and its stored energy will increase by $\mathbb{E}[E(P_m)]$. Following from the normalization in (25), this increase results in a definite transition (with probability 1) from state S_i to state S_{i+1} . On the other hand, when $i \geq L$, R enters the EH mode when the S-D link is not in outage (with probability $1 - p_{SD}$) which will also move the chain from state S_i to the subsequent state S_{i+1} . For this range of values of i , the outage of the S-D link (with probability p_{SD}) will make R enter the IR mode and, hence, its stored energy will decrease by $\frac{P_m}{2} - \mathbb{E}[E(P_m/2)]$ which will move the chain to state S_{i-v} where v is defined in (27). The corresponding approximate discrete-space Markov chain is depicted in Fig. 3.

From (26) and Fig. 3, the steady-state balance equations can be written as:

$$\pi_i = 0 \quad ; \quad i = 0, \dots, L - v - 1 \quad (28)$$

$$\pi_i = \pi_{i-1} + p_{SD}\pi_{i+v} \quad ; \quad i = L - v, \dots, L \quad (29)$$

$$\pi_i = q_{SD}\pi_{i-1} + p_{SD}\pi_{i+v} \quad ; \quad i > L, \quad (30)$$

where $q_{SD} \triangleq 1 - p_{SD}$.

Proposition 2: For sufficiently large values of v , solving equations (28), (29) and (30) results in the following values of the steady-state probabilities $\{\pi_i ; i \geq L\}$:

$$\pi_i = \frac{1}{v+1} q_{SD}^{i-L} \quad ; \quad i \geq L, \quad (31)$$

where, from (27), large values of v arise when the harvested energy is much smaller than the transmitted energy.

Proof: The proof is provided in Appendix B. ■

The probabilities in (31) are useful for evaluating the system outage probability in closed-form. In fact, the probability that the energy buffer contains a sufficient amount of energy for data relaying can be determined from (31) as follows:

$$\Pr(B \geq P_m/2) = \sum_{i=L}^{+\infty} \pi_i = \frac{q_{SD}^{-L}}{v+1} \sum_{i=L}^{+\infty} q_{SD}^i = \frac{1}{p_{SD}(v+1)}. \quad (32)$$

Replacing (32) in (9) shows that the system outage probability can be evaluated as follows:

$$P_{out} = p_{SD} - \frac{1}{v+1} [1 - p_{SR}] [1 - p_{RD}], \quad (33)$$

where the parameter v captures the performance dependence on the average amounts of transmitted and harvested energies according to (27).

Equation (33) clearly highlights a reduction in the outage probability compared to noncooperative point-to-point communications (along the S-D link). Note that v decreases as the amount of harvested energy increases resulting in a decrease in the value of P_{out} following from (33).

IV. NUMERICAL RESULTS

The simulation parameters are summarized in Table I. In particular, we consider the cases of “clear air”, “haze”, “moderate rain” and “light fog” weather conditions that affect the attenuation levels and turbulence-induced losses. Further details on the simulation parameters can be found in [5], [21], [26]. In all presented simulation scenarios, the distances between the nodes are selected to satisfy the relation $d_2 + d_3 = d_1$. Regarding the noise, considering a noise standard deviation of 10^{-7} A and a transmission bandwidth of 1 GHz (which both constitute typical values for FSO systems [26]), results in a noise power spectral density of -140 dBm/MHz. Finally, we assume the same pointing error conditions along all links.

Results in Fig. 4 show a perfect match between the exact pdf and the approximate analytical expression provided in (14) under different weather conditions for a link distance of 500 m with $\omega_z/a = 10$. Therefore, the approximation made in Appendix A induces no loss in the accuracy. Results also highlight on the small levels of harvested energy especially under unfavourable weather conditions. Under “clear air” conditions, the standard deviation of the harvested energy is equal to 12.8 mJ. Under “haze” and “moderate rain” conditions, the standard deviation drops to 5.5 mJ and 3.4 mJ, respectively. Under “light fog” conditions, the standard deviation assumes the smallest value of 1.1 mJ. The observed small values of the standard deviation of the harvested energy support observation

TABLE I
THE SIMULATION PARAMETERS

FSO parameters		
Operating Wavelength (λ)	1550 nm	
Receiver Responsivity (η)	0.5 A/W	
Transmission Bandwidth	1 GHz	
Peak Transmitted Power (P_m)	100 mW	
Noise standard deviation (σ)	10^{-7} A	
Receiving Area (S_r)	0.05 m ²	
Beam Angle (θ_d)	10 mrad	
Normalized pointing error displacement standard deviation (σ_s/a)	3	
EH parameters		
Fill factor (f)	0.75	
Dark saturation current (I_0)	10^{-9} A	
Thermal voltage (V_t)	25 mV	
Weather-dependent parameters		
Weather Condition	Attenuation coefficient (σ_a)	Refractive-index structure parameter (C_n^2)
Clear air	0.43 dB/km	$5 \times 10^{-14} \text{ m}^{-2/3}$
Haze	4.2 dB/km	$1.7 \times 10^{-14} \text{ m}^{-2/3}$
Moderate Rain (12.5 mm/hr)	11 dB/km	$5 \times 10^{-15} \text{ m}^{-2/3}$
Light Fog	20 dB/km	$3 \times 10^{-15} \text{ m}^{-2/3}$

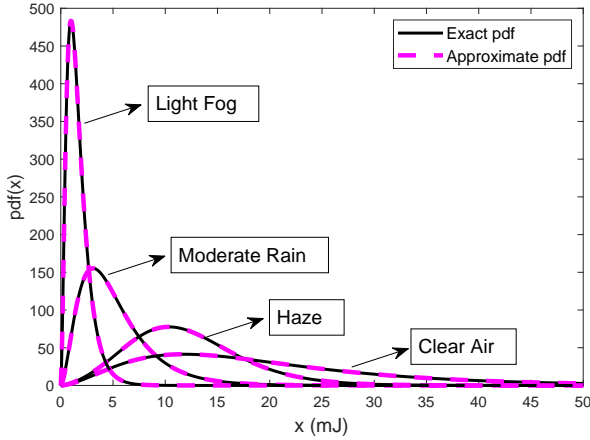


Fig. 4. PDF of the harvested energy for a link distance of 500 m with $\omega_z/a = 10$ under different weather conditions. The solid and dashed lines correspond to the exact pdf and approximate pdf (provided in (14)), respectively.

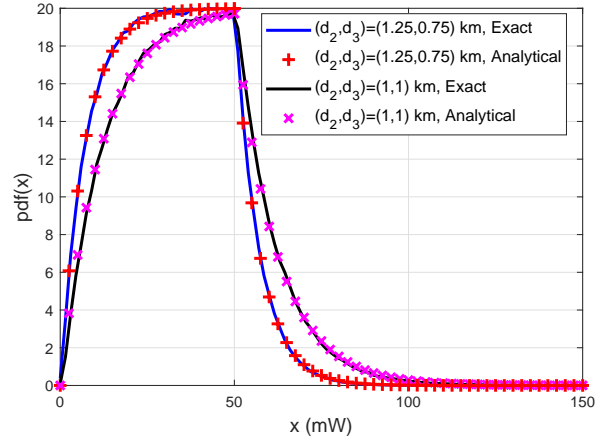


Fig. 5. Limiting pdf of the energy buffer content under “clear air” conditions for $R_{th} = 4$ bits/s/Hz with $\omega_z/a = 25$. The analytical expression of the pdf is provided in (11).

1 and motivate the calculation methodology presented in Section III-D. The standard deviation will further decrease as the distance increases.

In Fig. 5, we investigate the energy buffer content under “clear air” conditions for a threshold rate of $R_{th} = 4$ bits/s/Hz with $\omega_z/a = 25$. In particular, we compare the exact pdf of the energy buffer content with the analytical result derived in (11)-(13) for the two cases $(d_2, d_3) = (1.25, 0.75)$ km and $(d_2, d_3) = (1, 1)$ km. Results demonstrate the close match between the exact and analytical results, thus, validating the suggested exponential model of the energy buffer distribution under gamma-gamma scintillation and pointing errors. As highlighted in (11), the limit between the increasing and decreasing regions of the pdf occurs at $\frac{P_m}{2} = 50$ mW. Comparing the two considered cases shows that the energy buffer content

will tend to smaller stored energy levels in case 1 since the S-R link is longer resulting in smaller amounts of harvested energy. This is validated by the decrease of the value of the parameter b from 0.144 mW^{-1} in case 1 to 0.085 mW^{-1} in case 2 in coherence with (13). Finally, it is worth highlighting that the limiting distribution exists in both cases since the left-hand-side and right-hand-side of the inequality in (10) are equal to (2.3, 21.6) mW and (3.9, 21.6) mW for case 1 and case 2, respectively.

Fig. 6 shows the outage performance as a function of the target threshold rate R_{th} under “moderate rain” conditions for $\omega_z/a = 10$ considering the two scenarios $(d_2, d_3) = (0.3, 0.7)$ km and $(d_2, d_3) = (0.35, 0.65)$ km. As a benchmark, we also show the performance of the 1-km direct S-D communications with no cooperation and that of the cooperative network with

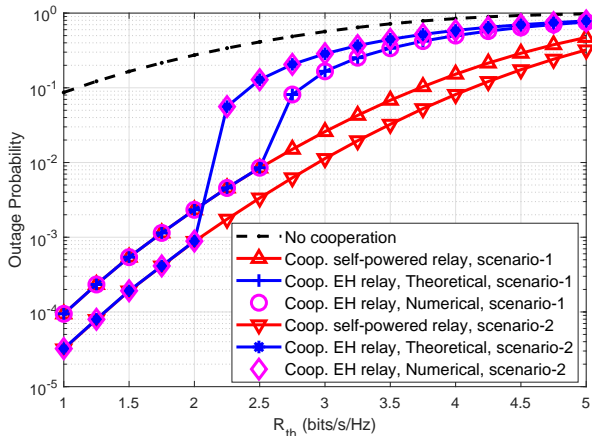


Fig. 6. Outage performance under “moderate rain” conditions for $\omega_z/a = 10$. Scenario-1 corresponds to $(d_2, d_3) = (0.3, 0.7)$ km while scenario-2 corresponds to $(d_2, d_3) = (0.35, 0.65)$ km. The theoretical results are based on (9) and (15).

a self-powered relay that is connected to a power supply. Results show the perfect match between the simulation results and the theoretical results obtained from (9) where the energy outage probability $\Pr(B < P_m/2)$ was derived according to (15) based on the continuous approach. Results show that the considered relaying scheme with an EH relay outperforms noncooperative systems for all values of R_{th} . For example, at a rate of 2 bits/s/Hz, the cooperative solution through an EH relay reduces the outage probability from 3×10^{-1} to 2×10^{-3} in scenario-1. Moreover, for relatively small values of R_{th} , the outage probability with an EH relay approaches the outage probability with a self-powered relay. In fact, when R_{th} is small, p_{SD} is small as well implying that R can harvest a sufficient amount of energy since R is in the pure EH mode with probability $1 - p_{SD}$. For scenario-1, results show that the inequality in (10) does not hold for $R_{th} \leq 2.5$. Consequently, in this case, the performance is the same with an EH relay or self-powered relay since the stored energy will exceed $\frac{P_m}{2}$ with a probability tending to 1 as highlighted in Section III-B. For $R_{th} > 2.5$, using only the energy harvested from S for relaying the information to D will incur a performance loss compared to the case where R is connected to a power supply. For scenario-2, results show that the inequality in (10) holds for all values of R_{th} exceeding 2. In this case, the higher losses along the longer S-R link result in lower levels of harvested energy thus avoiding the saturation of the energy buffer at R.

Fig. 7 highlights the impact of the relay position on the outage performance under “haze” conditions for $d_1 = 1.6$ km, $R_{th} \in \{1, 2, 3\}$ bits/s/Hz and $\omega_z/a = 25$. For a self-powered relay, placing the relay at the center between S and D (i.e. $d_2 = d_3 = 0.8$ km) minimizes P_{out} . On the other hand, for an EH relay, moving R closer to S results in two contradictory effects. On one hand, this will boost the energy harvesting at R thus reducing the probability of energy outage (the term $\Pr(B < P_m/2)$ in (9)) while the discrepancy between the values of d_2 and d_3 will increase the term $p_{SR} + p_{RD} - p_{SR}p_{RD} \approx \max\{p_{SR}, p_{RD}\}$ in (9). Consequently,

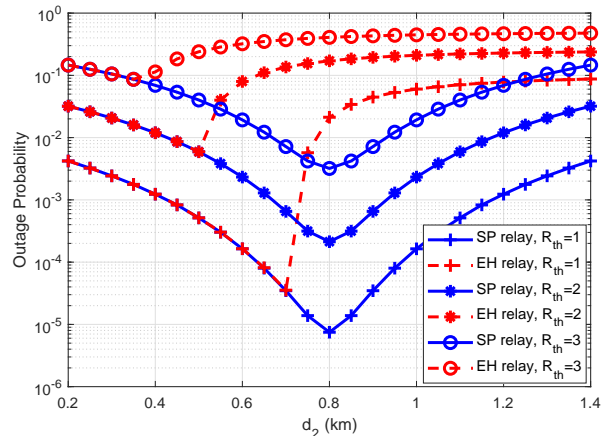


Fig. 7. Impact of the relay position on the performance under “haze” conditions for $d_1 = 1.6$ km and $\omega_z/a = 25$. The solid and dashed lines correspond to EH relay and self-powered (SP) relay, respectively.

a tradeoff must be made on the value of d_2 . As shown in Fig. 7, the optimal relay position shifts more towards S as R_{th} increases since, in this case, p_{SD} increases and R is in the IR mode more often thus draining the energy buffer at a faster pace. In order to compensate for this effect, R needs to be placed closer to S to increase the amount of harvested energy. For example, for $R_{th} = 1$ bits/s/Hz, P_{out} is minimized for $d_1 = 0.7$ km while this value decreases to 0.5 km for $R_{th} = 2$ bits/s/Hz.

Fig. 8 compares the different approaches for studying the buffer dynamics under “clear air” conditions for the two cases $d_2 = d_3 = 1$ km and $d_2 = d_3 = 1.2$ km with $\omega_z/a \rightarrow \infty$ (i.e. negligible pointing errors). In particular, we compare the continuous approach, exact discrete approach and approximate discrete approach presented in sections III-B, III-C and III-D, respectively. For the latter approach, we approximate the transition probabilities in (16)-(23) by the approximate values in (26) while using the expression in (24) for deriving the steady-state distribution. According to observation 1, the approximate discrete approach is expected to yield accurate results in the two simulation setups since the standard deviation of the harvested energy is equal to 5.3 mW and 3.8 mW in case 1 and case 2, respectively. In addition to the above three approaches, in Fig. 8 we also plot the closed-form expression provided in (33). The parameter v in (27) assumes the values of $v = 8$ and $v = 13$ for case 1 and case 2, respectively, where these values are large enough for proposition 2 to hold. Therefore, (33) is also expected to yield accurate results. Finally, for the discrete Markov chain, we fix the total number of states to $L' = 5000$ for both the exact and approximate approaches. Results in Fig. 8 show that the Markov state space discretization yields satisfactory results whose accuracy enhances as R_{th} increases. Moreover, the gap between the exact and approximate discrete approaches is negligible thus supporting the calculation methodology presented in Section III-D. Finally, results demonstrate the importance of the simple and closed-form expression in (33) for predicting the system performance through the parameter v

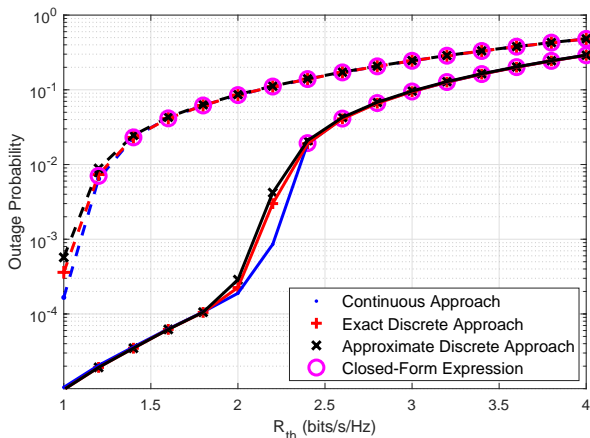


Fig. 8. The different calculation methodologies under “clear air” conditions for $\omega_z/a \rightarrow \infty$. The solid and dashed lines correspond to the cases $d_2 = d_3 = 1$ km and $d_2 = d_3 = 1.2$ km, respectively. The *closed-form expression* corresponds to (33).

that depends on the transmitted energy as well as the average values of the harvested energy. In this context, it is worth noting that the exact and approximate discrete approaches yield accurate results whether (10) holds or not while (33) holds for stable energy buffers.

While the peak power P_m was fixed to 100 mW in all previous figures, Fig. 9 highlights on the impact of P_m on the outage performance under “light fog” conditions for $d_2 = 0.4$ km and $d_3 = 0.3$ km with $\omega_z/a = 10$. Results show a rapid decrease in the outage probability as P_m increases especially for small values of R_{th} . As in Fig. 8, results in Fig. 9 highlight on the accuracy of the closed-form expression in (33) in predicting the system performance.

V. CONCLUSION

We proposed a novel relaying scheme for DF HSU FSO cooperative communications with a single relay. An analytical framework was presented for evaluating the system performance in both an exact manner as well as in a simple approximate closed-form manner. Results show that when sufficient amounts of energy are harvested, the considered scheme achieves the same outage probability as with self-powered relays. For smaller amounts of harvested energy, the proposed scheme always shows an improvement compared to point-to-point noncooperative communications. The impacts of the weather conditions, link distances and transmit power were delineated and conclusions were made pertaining to the optimal placement of the EH-relay.

APPENDIX A

The cdf and pdf of the random variable X will be denoted by $F_X(\cdot)$ and $f_X(\cdot)$, respectively. We first start by deriving the pdf of the harvested energy in (6). Equations (6)-(7) can be written as $E = \mu h \ln(1 + \frac{h}{\nu})$ where the constants μ and ν are defined in proposition 1 while $h = h_2$ for simplicity. The dark saturation current I_0 in (6) is typically very small (in the order of nA) [5] implying that E can be approximated by

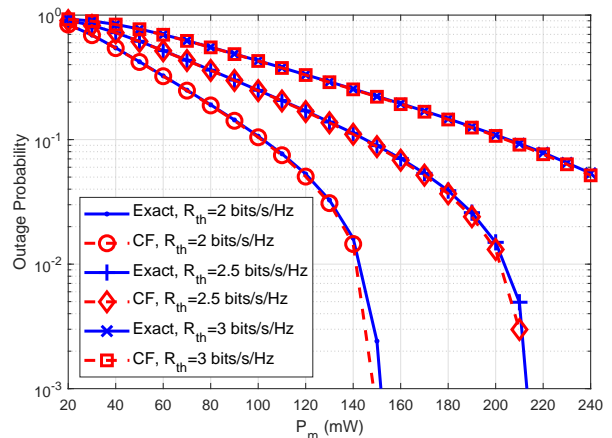


Fig. 9. Impact of the transmit peak power on the performance under “light fog” conditions for $d_2 = 0.4$ km and $d_3 = 0.3$ km with $\omega_z/a = 10$. The *closed-form expression* (CF) corresponds to (33).

$E = \mu h \ln(\frac{h}{\nu})$ without any loss of accuracy. Let $h' = \ln(\frac{h}{\nu})$, then $E = \mu \nu h' e^{h'}$. Consequently, $F_E(x) = \Pr(E \leq x) = \Pr(h' e^{h'} \leq \frac{x}{\mu \nu}) = \Pr(h' \leq W(\frac{x}{\mu \nu}))$ since the Lambert W-function $W(x)$ is the inverse function of $x e^x$. Consequently, $F_E(x) = F_{h'}(W(\frac{x}{\mu \nu}))$. Differentiating both sides of this equation while invoking the differentiation property of the Lambert W-function results in:

$$f_E(x) = \frac{W(\frac{x}{\mu \nu})}{[W(\frac{x}{\mu \nu}) + 1] x} f_{h'}\left(W\left(\frac{x}{\mu \nu}\right)\right). \quad (34)$$

On the other hand, $F_{h'}(x) = \Pr(h' \leq x) = \Pr(h \leq \nu e^x) = F_h(\nu e^x)$. Differentiating both sides of this equation results in:

$$f_{h'}(x) = \nu e^x f_h(\nu e^x), \quad (35)$$

where $f_h(\cdot)$ stands for the pdf of the random variable h given in (3) with $i = 1$. Finally, substituting (35) in (34) results in the pdf provided in (14) following from the relation $W(x)e^{W(x)} = x$.

Setting $B(i+1) = X$ and $B(i) = U$, then (8) can be written as:

$$X = \begin{cases} U + E' - M, & \text{S-D link in outage \& } U \geq M; \\ U + E, & \text{otherwise.} \end{cases}, \quad (36)$$

where $M \triangleq P_m/2$, $E \triangleq E(P_m)$ and $E' \triangleq E(P_m/2)$ for simplicity. From (6)-(7), it can be observed that E' can be obtained from E by replacing the scintillation coefficient h by $h/2$ (while keeping the same value of P_m). Consequently, $F_{E'}(x) = F_E(2x)$ and $f_{E'}(x) = 2f_E(2x)$.

From (36), the cdf of X can be obtained as:

$$\Pr(X \leq x) = \underbrace{\Pr(U + E' - M \leq x, U \geq M, \text{SD in outage})}_{=P_1} + \underbrace{\Pr(U + E \leq x, U < M)}_{=P_2} + \underbrace{\Pr(U + E \leq x, U \geq M, \text{SD not in outage})}_{=P_3}. \quad (37)$$

The pdf and cdf of U will be denoted by $g(u)$ and $G(u)$, respectively, with:

$$(g(u), G(u)) = \begin{cases} (g_1(u), G_1(u)), & 0 \leq u < M; \\ (g_2(u), G_2(u)), & u \geq M. \end{cases} \quad (38)$$

Through direct calculations, P_1 can be determined from:

$$\begin{aligned} P_1 &= p_{\text{SD}} \int_M^{M+x} F_{E'}(x-u+M)g_2(u)du \\ &= p_{\text{SD}} \int_M^{M+x} F_E(2x-u+M)g_2(u)du, \end{aligned} \quad (39)$$

where, from (38), the pdf of U was replaced by $g_2(u)$ since $U \geq M$. Similarly:

$$P_2 = \int_0^{\min\{x, M\}} F_E(x-u)g_1(u)du, \quad (40)$$

where, from (38), the pdf of U was replaced by $g_1(u)$ since $U < M$. Finally:

$$P_3 = \begin{cases} 0, & x < M; \\ (1-p_{\text{SD}}) \int_M^x F_E(x-u)g_2(u)du, & x \geq M. \end{cases} \quad (41)$$

When the energy buffer reaches its steady-state, $f_X(\cdot) = f_U(\cdot) \rightarrow g(\cdot)$ and $F_X(\cdot) = F_U(\cdot) \rightarrow G(\cdot)$ which corresponds to the limiting distribution. Therefore, at steady-state, considering the cases $x < M$ and $x \geq M$ separately, (37) can be written as:

$$\begin{aligned} G_1(x) &= \int_0^x F_E(x-u)g_1(u)du \\ &\quad + p_{\text{SD}} \int_M^{M+x} F_E(2x-u+M)g_2(u)du, \end{aligned} \quad (42)$$

$$\begin{aligned} G_2(x) &= \int_0^M F_E(x-u)g_1(u)du \\ &\quad + (1-p_{\text{SD}}) \int_M^x F_E(x-u)g_2(u)du \\ &\quad + p_{\text{SD}} \int_M^{M+x} F_E(2x-u+M)g_2(u)du. \end{aligned} \quad (43)$$

Differentiating (42) and (43) with respect to x results in:

$$\begin{aligned} g_1(x) &= \int_0^x f_E(x-u)g_1(u)du \\ &\quad + 2p_{\text{SD}} \int_M^{M+x} f_E(2x-u+M)g_2(u)du, \end{aligned} \quad (44)$$

$$\begin{aligned} g_2(x) &= \int_0^M f_E(x-u)g_1(u)du \\ &\quad + (1-p_{\text{SD}}) \int_M^x f_E(x-u)g_2(u)du \\ &\quad + 2p_{\text{SD}} \int_M^{M+x} f_E(2x-u+M)g_2(u)du, \end{aligned} \quad (45)$$

where the pdf $f_E(x)$ of the harvested energy is given in (14). Subtracting (44) from (45):

$$\begin{aligned} g_2(x) - g_1(x) &= \int_x^M f_E(x-u)[g_1(u) - \bar{p}_{\text{SD}}g_2(u)]du \\ &= - \int_0^{x-M} f_E(t)[g_1(x-t) - \bar{p}_{\text{SD}}g_2(x-t)]dt, \end{aligned} \quad (46)$$

where $\bar{p}_{\text{SD}} \triangleq 1 - p_{\text{SD}}$. By numerically observing the exponential charging and discharging of the energy buffer, we postulate a solution for (46) under the form $g_1(x) = a[1 - e^{-bx}]$ (exponential charging) and $g_2(x) = ce^{-bx}$ (exponential discharging) as highlighted in (11). We then prove that the suggested solution satisfies all buffer dynamics equations and, hence, constitutes the valid steady-state distribution we are seeking. Replacing $g_1(x)$ and $g_2(x)$ in (46) results in:

$$\begin{aligned} -a + (a+c)e^{-bx} &= \\ -a \int_0^{x-M} f_E(t)dt + (a + \bar{p}_{\text{SD}}c)e^{-bx} \int_0^{x-M} f_E(t)e^{bt}dt. \end{aligned} \quad (47)$$

Equation (47) holds for all values of x . In particular, for sufficiently large values of x , $\int_0^{x-M} f_E(t)dt \rightarrow \int_0^{+\infty} f_E(t)dt = 1$ since $f_E(t)$ is a pdf. Consequently, for large values of x , (47) implies that:

$$(a+c)e^{-bx} = (a + \bar{p}_{\text{SD}}c)e^{-bx} \int_0^{+\infty} f_E(t)e^{bt}dt, \quad (48)$$

implying that:

$$\frac{a+c}{a + \bar{p}_{\text{SD}}c} = \int_0^{+\infty} f_E(t)e^{bt}dt. \quad (49)$$

The two remaining equations needed to solve for a , b and c follow from the following conditions. (i): $g(x)$ is a pdf implying that $\int_0^{+\infty} g(x)dx = \int_0^M g_1(x)dx + \int_M^{+\infty} g_2(x)dx = 1$. (ii): The continuity of the pdf at the point $x = M$ results in $g_1(M) = g_2(M)$. After simplification, the obtained equations result in:

$$a \left[M - \frac{1}{b} \right] + \frac{a+c}{b} e^{-bM} = 1, \quad (50)$$

$$e^{-bM} = \frac{a}{a+c}. \quad (51)$$

Replacing $a+c$ by ae^{bM} in (50) results in $a = \frac{1}{M} = \frac{2}{P_n}$ as provided in (12). Replacing this value of a in (51) results in $c = a[e^{bM} - 1]$ as provided in (12). Finally, replacing a and c by their values in (49) results in (13).

APPENDIX B

We first consider the first v equations in (29) for $i = L-v, \dots, L-1$. Replacing the value of π_i in the $(i+1)$ -th equation shows that these v equations can be written under the following more convenient form:

$$\pi_{L-(v-j)} = p_{\text{SD}} \sum_{k=0}^j \pi_{L+k} \quad ; \quad j = 0, \dots, v-1. \quad (52)$$

Next, we consider the $(v+1)$ -th equation in (29) (for $i = L$) that can be written as: $\pi_L = \pi_{L-1} + p_{\text{SD}}\pi_{L+v}$. Replacing the value of π_{L-1} from (52) (for $j = v-1$) in the last equation results in:

$$\pi_L = p_{\text{SD}} \sum_{k=0}^{v-1} \pi_{L+k} + p_{\text{SD}}\pi_{L+v} = p_{\text{SD}} \sum_{k=0}^v \pi_{L+k}. \quad (53)$$

Solving (53) for π_L results in:

$$\pi_L = \frac{p_{\text{SD}}}{q_{\text{SD}}} [\pi_{L+1} + \dots + \pi_{L+v}]. \quad (54)$$

The recursive replacement of (54) in (30) shows that the last set of equations results in:

$$\pi_i = \frac{p_{SD}}{q_{SD}} \sum_{j=1}^v \pi_{i+j} \quad ; \quad i \geq L. \quad (55)$$

We suggest a solution for (55) under the form:

$$\pi_i = \alpha q_{SD}^i \quad ; \quad i \geq L, \quad (56)$$

and next we prove that this solution holds if v is large enough. In (56), α denotes a proportionality constant. Replacing (56) in (55):

$$\alpha q_{SD}^i = \alpha \frac{p_{SD}}{q_{SD}} q_{SD}^i \sum_{j=1}^v q_{SD}^j = \alpha p_{SD} q_{SD}^i \sum_{j=0}^{v-1} q_{SD}^j. \quad (57)$$

The summation in (57) corresponds to a geometric series that can be solved as $\sum_{j=0}^{v-1} q_{SD}^j = \frac{1-q_{SD}^v}{1-q_{SD}}$ that tends to $\frac{1}{1-q_{SD}} = \frac{1}{p_{SD}}$ if $v \gg 1$ so that $q_{SD}^v \rightarrow 0$ since $q_{SD} < 1$. Replacing the last summation by $\frac{1}{p_{SD}}$ in (57) results in $\alpha q_{SD}^i = \alpha q_{SD}^i$ which is true. Consequently, the proposed solution in (56) is correct for $v \gg 1$.

Finally, the value of the constant α in (56) can be obtained by solving the equation $\sum_{i=0}^{+\infty} \pi_i = 1$. This equation can be written as:

$$\underbrace{\sum_{i=0}^{L-v-1} \pi_i}_{\triangleq S_1} + \underbrace{\sum_{i=L-v}^{L-1} \pi_i}_{\triangleq S_2} + \underbrace{\sum_{i=L}^{+\infty} \pi_i}_{\triangleq S_3} = 1. \quad (58)$$

Form (28), $S_1 = 0$. From (56), $\frac{S_3}{\alpha} = \sum_{i=L}^{+\infty} q_{SD}^i = \frac{q_{SD}^L}{p_{SD}}$ through direct calculations. From (52):

$$\begin{aligned} S_2 &= p_{SD} \sum_{j=0}^{v-1} \sum_{k=0}^j \pi_{L+k} \\ &= p_{SD} [v\pi_L + (v-1)\pi_{L+1} + \dots + \pi_{L+v-1}] \\ &= p_{SD} \sum_{i=0}^{v-1} (v-i)\pi_{L+i} = \alpha p_{SD} q_{SD}^L \sum_{i=0}^{v-1} (v-i)q_{SD}^i, \quad (59) \end{aligned}$$

where the second equality in (59) follows from (56). The last summation in (59) can be solved through direct calculations resulting in $S_2 = \alpha p_{SD} q_{SD}^L \left[\frac{v}{p_{SD}} - \frac{q_{SD}^v}{p_{SD}} \right]$. Replacing the values of S_1 , S_2 and S_3 in (58) and solving for α results in: $\alpha = \frac{1}{q_{SD}^L(v+1)}$. Finally, replacing α by its value in (56) results in the solution given in (31).

REFERENCES

- [1] M. Safari and M. Uysal, "Relay-assisted free-space optical communication," *IEEE Trans. Wireless Commun.*, vol. 7, no. 12, pp. 5441–5449, Dec. 2008.
- [2] S. Bi, Y. Zeng, and R. Zhang, "Wireless powered communication networks: An overview," *IEEE Wireless Commun.*, vol. 23, no. 2, pp. 10–18, Apr. 2016.
- [3] M. A. Hossain, R. M. Noor, K.-L. A. Yau, I. Ahmedy, and S. S. Anjum, "A survey on simultaneous wireless information and power transfer with cooperative relay and future challenges," *IEEE Access*, vol. 7, pp. 19 166–19 198, Feb. 2019.
- [4] X. Zhou, R. Zhang, and C. K. Ho, "Wireless information and power transfer: Architecture design and rate-energy tradeoff," *IEEE Trans. Commun.*, vol. 61, no. 11, pp. 4754–4767, Nov. 2013.

- [5] P. D. Diamantoulakis, G. K. Karagiannidis, and Z. Ding, "Simultaneous lightwave information and power transfer (SLIPT)," *IEEE Trans. on Green Commun. and Networ.*, vol. 2, no. 3, pp. 764–773, Sep. 2018.
- [6] R. Morsi, D. S. Michalopoulos, and R. Schober, "On-off transmission policy for wireless powered communication with energy storage," in *2014 48-th Asilomar Conference on Signals, Systems and Computers*, 2014, pp. 1676–1682.
- [7] —, "Performance analysis of wireless powered communication with finite/infinite energy storage," in *2015 IEEE International Conference on Communications (ICC)*, June 2015, pp. 2469–2475.
- [8] D. Bapatla and S. Prakriya, "Performance of energy-buffer aided incremental relaying in cooperative networks," *IEEE Trans. Wireless Commun.*, vol. 18, no. 7, pp. 3583–3598, July 2019.
- [9] —, "Performance of a cooperative network with an energy buffer-aided relay," *IEEE Trans. on Green Commun. and Networ.*, vol. 3, no. 3, pp. 774–788, Sep. 2019.
- [10] I. Krikidis, S. Timotheou, and S. Sasaki, "RF energy transfer for cooperative networks: Data relaying or energy harvesting?" *IEEE Commun. Lett.*, vol. 16, no. 11, pp. 1772–1775, Nov. 2012.
- [11] I. Krikidis, "Relay selection in wireless powered cooperative networks with energy storage," *IEEE J. Select. Areas Commun.*, vol. 33, no. 12, pp. 2596–2610, Dec. 2015.
- [12] Y. Gu, H. Chen, Y. Li, Y.-C. Liang, and B. Vucetic, "Distributed multi-relay selection in accumulate-then-forward energy harvesting relay networks," *IEEE Trans. on Green Commun. and Networ.*, vol. 2, no. 1, pp. 74–86, Mar. 2017.
- [13] K.-H. Liu, "Performance analysis of relay selection for cooperative relays based on wireless power transfer with finite energy storage," *IEEE Trans. Veh. Technol.*, vol. 65, no. 7, pp. 5110–5121, July 2015.
- [14] D. Wang, P. Ren, and J. Cheng, "Cooperative secure communication in two-hop buffer-aided networks," *IEEE Trans. Commun.*, vol. 66, no. 3, pp. 972–985, Mar. 2017.
- [15] J. Ouyang, Y. Che, J. Xu, and K. Wu, "Throughput maximization for laser-powered UAV wireless communication systems," in *2018 IEEE Int. Conf. on Commun. Workshops*, May 2018, pp. 1–6.
- [16] B. Makki, T. Svensson, K. Buisman, J. Perez, and M.-S. Alouini, "Wireless energy and information transmission in FSO and RF-FSO links," *IEEE Wireless Commun. Letters*, vol. 7, no. 1, pp. 90–93, Feb. 2017.
- [17] G. Pan, P. D. Diamantoulakis, Z. Ma, Z. Ding, and G. K. Karagiannidis, "Simultaneous lightwave information and power transfer: Policies, techniques, and future directions," *IEEE Access*, vol. 7, pp. 28 250–28 257, Mar. 2019.
- [18] C. Abou-Rjeily, G. Kaddoum, and G. K. Karagiannidis, "Ground-to-air FSO communications: when high data rate communication meets efficient energy harvesting with simple designs," *OSA Optics Express*, vol. 27, no. 23, pp. 34 079–34 092, Nov. 2019.
- [19] H.-V. Tran, G. Kaddoum, P. D. Diamantoulakis, C. Abou-Rjeily, and G. K. Karagiannidis, "Ultra-small cell networks with collaborative RF and lightwave power transfer," *IEEE Trans. Commun.*, vol. 67, no. 9, pp. 6243–6255, Sep. 2019.
- [20] P. D. Diamantoulakis, K. N. Pappi, Z. Ma, X. Lei, P. C. Sofotasios, and G. K. Karagiannidis, "Airborne radio access networks with simultaneous lightwave information and power transfer (SLIPT)," in *IEEE Global Commun. Conf.*, 2018, pp. 1–6.
- [21] B. Zhu, J. Cheng, and L. Wu, "A distance-dependent free-space optical cooperative communication system," *IEEE Commun. Lett.*, vol. 19, no. 6, pp. 969–972, June 2015.
- [22] H. Sandalidis, T. Tsiftsis, and G. Karagiannidis, "Optical wireless communications with heterodyne detection over turbulence channels with pointing errors," *J. Lightwave Technol.*, vol. 27, no. 20, pp. 4440–4445, October 2009.
- [23] A. Lapidith, S. M. Moser, and M. A. Wigger, "On the capacity of free-space optical intensity channels," *IEEE Trans. Inform. Theory*, vol. 55, no. 10, pp. 4449–4461, Oct. 2009.
- [24] N. D. Chatzidiamantis, D. S. Michalopoulos, E. E. Kriezis, G. K. Karagiannidis, and R. Schober, "Relay selection protocols for relay-assisted free-space optical systems," *IEEE J. Opt. Commun. Netw.*, vol. 5, no. 1, pp. 4790–4807, January 2013.
- [25] M.-M. Zhao, Q. Shi, and M.-J. Zhao, "Efficiency maximization for UAV-enabled mobile relaying systems with laser charging," *IEEE Trans. Wireless Commun.*, 2020, Early Access Article.
- [26] B. He and R. Schober, "Bit-interleaved coded modulation for hybrid RF/FSO systems," *IEEE Trans. Commun.*, vol. 57, no. 12, pp. 3753–3763, Dec. 2009.